A Pseudo-Rigid-Body Model for Large Deflections of Fixed-Clamped Carbon Nanotubes

Larry L. Howell
Department of Mechanical Engineering,
Brigham Young University,
Provo, UT 84602

Christopher M. DiBiasio

Michael A. Cullinan

Robert M. Panas

Martin L. Culpepper

Department of Mechanical Engineering,
Massachusetts Institute of Technology,
Cambridge, MA 02139

Carbon nanotubes (CNTs) may be used to create nanoscale compliant mechanisms that possess large ranges of motion relative to their device size. Many macroscale compliant mechanisms contain compliant elements that are subjected to fixed-clamped boundary conditions, indicating that they may be of value in nanoscale design. The combination of boundary conditions and large strains yield deformations at the tube ends and strain stiffening along the length of the tube, which are not observed in macroscale analogs. The large-deflection behavior of a fixed-clamped CNT is not well-predicted by macroscale large-deflection beam bending models or truss models. Herein, we show that a pseudo-rigid-body model may be adapted to capture the strain stiffening behavior and, thereby, predict a CNT's fixed-clamped behavior with less than 3% error from molecular simulations. The resulting pseudo-rigid-body model may be used to set initial design parameters for CNT-based compliant mechanisms. This removes the need for iterative, time-intensive molecular simulations during initial design phases. [DOI: 10.1115/1.4001726]

Keywords: compliant mechanism, pseudo-rigid-body, flexure, carbon nanotube, molecular simulations, nanomechanical, nanoelectromechanical

1 Introduction

This brief introduces a pseudo-rigid-body model (PRBM) that captures the large-deflection flexural behavior of a carbon nanotube (CNT) subject to a fixed-clamped boundary condition. This type of compliant element, shown in Fig. 1(*a*), is a ubiquitous building block of large-scale compliant mechanisms. For example, the flexure type show in Fig. 2 is composed of four fixed-clamped compliant elements and is commonly used to guide linear motion in macro- and microscale compliant mechanisms. A CNT-based version could be used in nanoscale force-displacement transducers [1], nanoscale sensors or actuators [2], resonators [3], memory [4], and switches [5].

Contributed by the Mechanisms and Robotics Committee of ASME for publication in the JOURNAL OF MECHANISMS AND ROBOTICS. Manuscript received August 12, 2008; final manuscript received April 6, 2010; published online July 14, 2010. Assoc. Editor: G. K. Ananthasuresh.

Figure 1 contrasts the fixed-clamped and fixed-guided boundary conditions. In a fixed-guided and a fixed-clamped beam, the ungrounded end is held at a constant angle. These end conditions are considered to be identical for small deflections but when deflections are large, they yield different kinematic and loading behaviors that result in different elastomechanic responses. Specifically, a fixed-clamped beam is subjected to an axial force $\mathbf{F_a}$, a bending force $\mathbf{F_b}$, and an end moment $\mathbf{M}$ while a fixed-guided beam is subjected only to a bending force and end moment. Fixed-clamped boundary conditions induce large axial stresses that cause a nonlinear stress stiffening effect during deformation. This increases the fixed-clamped beam's stiffness for larger deflections. The resulting stresses may make it infeasible to use fixed-clamped elements over large deflections via conventional materials. Thus, fixed-clamped elements have not received in-depth attention for large-deflection compliant mechanisms.

Understanding how to model nanoscale versions of the fixed-clamped elements during large deformations can enable the creation of unique nanomechanical systems. Herein, we focus on fixed-clamped CNTs because CNTs possess a combination of high elastic modulus ($\sim$1 TPa [6]) and exhibit large failure strains ($>$40% [7]). This combination makes possible the design of flexures with large stroke ($\sim$25% of device size) and high bandwidth ($\sim$GHz).

We will show that the large-deflection behavior of a fixed-clamped CNT is not well-predicted by conventional large-deflection beam bending models or by truss models. Molecular simulations are, therefore, required to obtain accurate kinematic and elastomechanic responses. This is problematic because molecular simulation may take days to complete. If the simulation finds that desired results are not obtained, the design must be adjusted and the simulation restarted. The combination of iteration and simulation time makes molecular simulations unsuitable for conceptual design.

The PRBM [8] provides an elegant and rapid means to perform initial assessment of a compliant mechanism's performance. In short, one finds a rigid-body mechanism that emulates the behavior of the compliant mechanism under consideration. The compliant mechanism may then be modeled as a rigid-link mechanism with torsional springs at each joint and analyzed using known rigid-link theory. The PRBM has been shown to be effective at modeling CNT-based parallel-guiding mechanisms [9], which consist of fixed-guided elements. The CNTs in this work did not experience strain stiffening, therefore, the model does not apply to fixed-clamped conditions. Herein, we present a new PRBM that captures the strain stiffening behavior and predicts the behavior of a (5,5) CNT with less than 3% error from molecular simulations. We present this specific case so that others may understand how to adapt PRBM to other types of CNTs, thereby, reducing iterative simulation time in early design.

2 Background

2.1 Previous Models of Fixed-Guided CNT Behavior. Previous work [10] has shown that large-displacement beam bending models are capable of predicting the behavior of fixed-clamped CNTs for displacements that are less than 7% of a CNT's length. Our simulations show that fixed-clamped (5,5) single-walled CNTs (SWCNTs) are capable of deformations that exceed 25% of their length. Macroscale, large-displacement models for fixed-clamped beams cannot accurately predict the elastomechanic behavior of these CNTs because of localized deformations that we found near the CNT's ends.

2.2 Overview of a CNT's Structure. The structure of a SWCNT may be visualized by rolling a graphene sheet into a cylinder. Basis vectors $\mathbf{a_1}$ and $\mathbf{a_2}$ define positions in the graphene sheet as shown in Fig. 3. The lattice of the graphene sheet may be

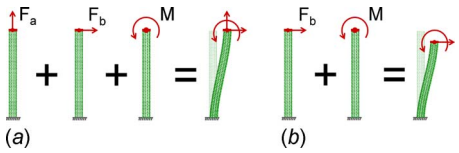

Fig. 1 Fixed-clamped (*a*) and fixed-guided element (*b*)

wrapped at many different chiral angles to form a CNT [11]. The magnitude of the chiral vector **c** defines the tube circumference in terms of basis vectors as

$$\mathbf{c} = n\mathbf{a}_1 + m\mathbf{a}_2 \tag{1}$$

where n and m are the chiral indices. The SWCNTs in this work were (5,5) tubes. Figure 3 highlights nanotube unit cells (NUCs) and a graphene unit cell, the two building blocks of a SWCNT. The NUC is repeated along the axis of the tube with period a. Given the complexity and number of compliant bonds between the carbon atoms, molecular simulations are typically used to ascertain interaction between atoms during deformation.

2.3 Molecular Mechanics Simulations. Although promising results have been obtained with finite element analysis (FEA) [12], these tools have yet to incorporate all phenomena that affect CNT behavior and it is uncertain if they will predict the localized deformations we observed during simulation. Molecular modeling has been shown to accurately predict the behavior of CNTs [13] and, therefore, it serves as our benchmark.

Molecular mechanics simulations treat a CNT as a collection of nodes (atoms) and compliant node-to-node connections that emulate atomic interactions. The molecular simulation's algorithm minimizes the system's total potential energy U_{total} by changing the length and orientation of the C–C bonds for a set of global forces. The total system potential contains contributions from several forms of bonded and nonbonded interactions.

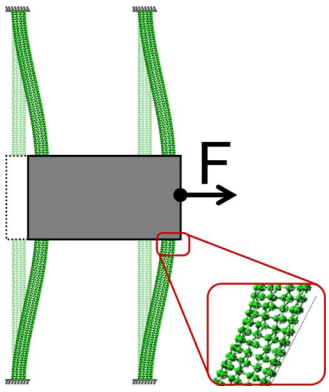

Fig. 2 A CNT–based linear motion flexure

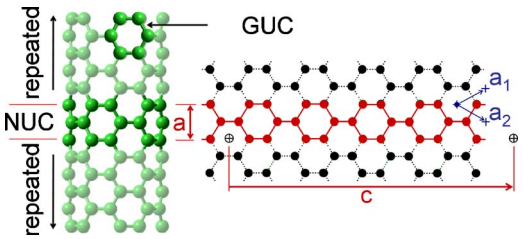

Fig. 3 Structure of a SWCNT

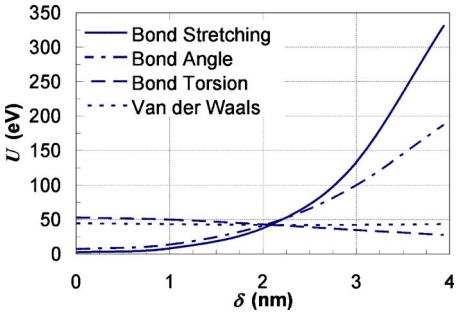

Fig. 4 Strain energy storage for CNT fixed-guided beams

$$U_{\text{total}} = \sum U_{B1} + \sum U_{B2} + \sum U_{B3} + \sum U_D + \sum U_{S-B} + \sum U_{vdW} \tag{2}$$

where U_{B1} is the contribution from bond stretching between atoms, U_{B2} is the contribution due to changes in the in-plane bond angle between atoms, U_{B3} is the energy stored via out-of plane bending of bonds, U_D is the energy stored in the dihedral (torsion) configuration of the bond, U_{S-B} is a stretch-bend correction term, and U_{vdW} is the energy from nonbonded van der Waals interactions.

3 Applicability of Macroscale Deformation Models

It is necessary to determine the amount of energy stored via nanoscale mechanisms, e.g., van der Waals interactions, relative to macroscalelike mechanisms such as bond stretching. Molecular mechanics simulations were conducted to quantify and provide insight into how energy U is stored over the CNT's range of motion. There are four primary modes of energy storage: (1) bond stretching, (2) bond angle deformation, (3) bond torsion, and (4) van der Waals interactions. As shown in Fig. 4, strain energy was stored primarily via stretching and angle rotations. The change via bond torsion and van der Waals forces was roughly 5% of that associated with stretching and angle rotations. The link between energy and stiffness indicates that bond torsions and van der Waals interactions contribute little to device stiffness. Our simulations show that this contribution was less than a 1% change in stiffness for a 7.64 nm long, (5,5), fixed-clamped CNT that was deflected in the lateral direction by 4 nm.

The effect of van der Waals generally decrease with increased tensile deformation because the nonbonded atoms in the aromatic rings move closer to the van der Waals equilibrium distance as the CNT is stretched [14]. These results indicate that it should be possible to model the fixed-clamped CNT beam via a macroscale model that captures strain stiffening behavior but does not include nanoscale effects. This conclusion is specific to the fixed-clamped elements. Nanoscale effects play important roles in the behavior of other CNT-based devices such as cantilevers [14] and fixed-guided elements [15].

4 Continuum Modeling of a CNT Fixed-Clamped Beam

Continuum models indicate that localized bending may occur in a fixed-clamped beam [16], however, most materials would plastically yield before this occurs. As such, these models have not seen use for our purpose. In these models, the deflection of the ungrounded tip is related to a load applied at the tip. One end of the beam is grounded while the other is constrained to move as shown in Fig. 1(*a*). The following subsections provide an overview of macroscale models that were considered as options for modeling CNTs. The results of each method will be compared with molecular simulation results and PRBM results.

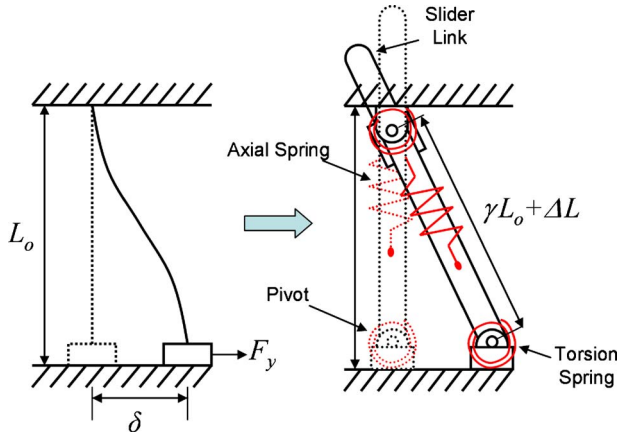

Fig. 5 Compliant element to rigid-link analogy

4.1 Large-Deflection Beam Bending Model. The Eulerian large-deflection model incorporates strain stiffening. The model [17] may be expressed mathematically as

$$(EI)_{\text{bending}}\frac{d^4y_A}{dx^4} - \frac{1}{2}(EA)_{\text{axial}}\frac{d^2y_A}{dx^2}\left(\frac{dy_A}{dx}\right)^2 = 0 \tag{3}$$

With fixed-clamped boundary conditions applied, the force-displacement relationship [17] is

$$F_y = \frac{\pi^4}{8L_o^3}(EI)_{\text{bending}}\delta + \frac{\pi^4}{128L_o^3}(EA)_{\text{axial}}\delta^3 \tag{4}$$

Equation (4) relates the applied load F_y to the displacement δ via beam length L_o flexural rigidity $(EI)_{\text{bending}}$ and force per unit strain $(EA)_{\text{axial}}$. A sinusoidal displacement profile [17] y_A was assumed as a function of position along the x as

$$y_A = \frac{\delta}{2}\left(1 + \cos\frac{\pi x}{L_o}\right) \quad \text{for} \quad 0 \le x \le L_o \tag{5}$$

4.2 Truss Model. A truss model was developed to provide a lower bound. This model assumes that the beam offers local axial resistance but no bending resistance. The results will not be accurate but they provide insight into the nature of the fixed-clamped CNT deformation. From these results it is possible to ascertain how much of the energy stored in the beam is due to axial stretching. The nonlinear stiffness k for the truss model is

$$k = \frac{(EA)_{\text{axial}}\delta^2}{(L_o^2 + \delta^2)^{3/2}} \tag{6}$$

5 PRBM for Fixed-Clamped Conditions

Previous work [9] has shown that PRB modeling may be used to accurately predict the large and nonlinear bending of CNT-based fixed-guided elements and their combination in a parallel-guiding mechanism. The previous work did not account for the longitudinal constraint and resulting stress stiffening. Figure 5 contains a fixed-clamped beam and its PRB equivalent. The locations of the pivots in the rigid mechanism are defined by a characteristic radius factor γ and the original beam length L_o. The required stiffness K_T of the torsion springs that emulate the beam's bending stiffness is

$$K_T = 2\frac{\gamma}{L_o}K_\theta(EI)_{\text{bending}} \tag{7}$$

where K_θ is the stiffness coefficient.

The axial stretching of the beam is modeled via a slider link with a linear spring. The nonlinear axial spring constant K_A is

$$K_A = \frac{(EA)_{\text{axial}}}{\gamma L_o + \Delta L} \tag{8}$$

where the increase in slider length ΔL is

$$\Delta L = \sqrt{\delta^2 + (\gamma L_o)^2} - \gamma L_o \tag{9}$$

The Poisson effect is important to the accuracy of these models. A 6% reduction in cross-sectional area was observed when the fixed-clamped CNT experienced an axial extension that correlated with a 4 nm transverse deflection of the CNT's tip. The cross-sectional area in Eq. (8) must be adjusted if the model is to predict the correct stiffness. This may be done by relating the cross-sectional area with increase in link length ΔL, the Poisson ratio, υ, the original diameter, D_o, and the wall thickness t.

$$A = \frac{\pi D_o t L_o\left(1 + \dfrac{\Delta L}{L_o}(1 - 2\nu)\right)}{L_o + \Delta L} \tag{10}$$

The principle of virtual work may be used to predict the elastomechanic response [8], yielding the following result:

$$F_y = \frac{K_A \Delta L \delta}{\Delta L + \gamma L_o} + \frac{2K_T\gamma L_o \tan^{-1}\left(\dfrac{\delta}{\gamma L_o}\right)}{(\Delta L + \gamma L_o)^2} \tag{11}$$

where K_T, K_A, and ΔL are defined in Eqs. (7) and (8), leaving δ as the independent variable.

The first term in Eq. (11) represents the component of force associated with an increase in the slider link's length. The second term represents the resistance to bending. For large deformations, the results of Eq. (11) are dominated by the first term. Herein, we apply this fixed-clamped PRBM to CNTs, however, this model is applicable to other materials and size regimes.

6 Results and Discussion

A simulation-based case study was used to compare the accuracy of the various methods. The case study was based upon the mechanism in Fig. 2. This device was chosen because it is an important flexural building block.

6.1 Molecular Model. The model was created from four (5,5) SWCNTs that were 7.64 nm long and 0.678 nm in diameter. The proximal ends were grounded and the distal ends were rigidly constrained to the stage. The stage was assumed to be rigid relative to the CNTs. This permitted a decoupled examination of the CNTs' behavior. An actuating force F was applied to the stage as shown in Fig. 2. Stage displacement were obtained via molecular simulations that utilized the MM+ force field and a Polak–Ribiere algorithm [18] that conducted optimization until a convergence criterion of 1 cal/mol Å had been reached.

6.2 Simulation and Model Results. The simulated elastomechanic response of the compliant mechanism is shown in Fig. 6. The forces applied in the continuum models for a single beam were modified according to $F=4F_y$ as the device is composed of four CNTs. For displacements less than 0.6 nm, the mechanism could be modeled with a constant stiffness of 2.1 N/m with less than 7.1% error. For displacements exceeding 0.6 nm, the mechanism experienced noticeable strain stiffening. At 4 nm (failure point) the stiffness was 31 N/m.

The results from Eq. (4) are plotted in Fig. 6 as "large deflection." The geometry and material property values used in Eq. (4) were selected from previous work [14] on CNT-based compliant mechanisms. Figure 6 shows that the force predictions of the large-deflection model are almost double the simulated values for displacements larger than 3 nm. The truss model's prediction in Fig. 6 show errors larger than 60% for small displacement, i.e., less than 1 nm. This model is more accurate than the large-

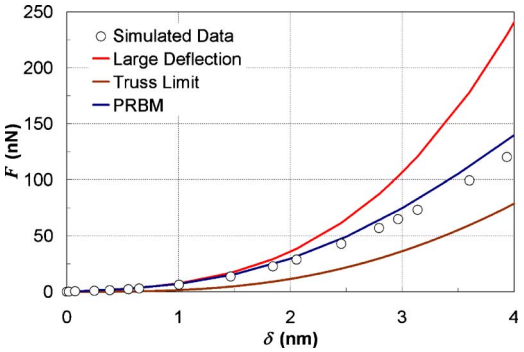

Fig. 6 Simulated and modeled elastomechanic response

deflection model when predicting stiffness at larger displacements. For example, the error in predicted stiffness beyond 4 nm is 91% in the large-deflection model and 18% in the truss model.

Figure 6 shows the PRBM's predictions versus the simulated data and predictions from the large-deflection model. Table 1 contains the values of the parameters used in the PRBM. The value of γ and K_θ were obtained from previous work [9]. Molecular simulations have been used to ascertain the values of $(EA)_{\text{axial}}$ and $(EI)_{\text{bending}}$ that enable accurate modeling of corresponding deformation modes in a (5,5) CNT [14]. For displacements less than 1 nm, the large-deflection model and PRBM predict stiffness within 10% of the simulated value. For displacements that are larger than 1 nm, the PRBM predicts required force to with less than 13% error while the maximum error for the "large beam deflection" model exceeds 90%.

6.3 Discussion of Results. The difference between continuum and simulation results may be understood by examination of Fig. 7. The simulated CNT shows two localized bending zones for displacements larger than 0.6 nm. The localized bending near the anchors defines the first zone while the second is defined by the axial deformation that occurs in the middle of the CNT. The localized behavior differs from the distributed deformation that is assumed within the beam profile for Eq. (5). We tried other beam profiles [16] but these models over predict the required force at full stroke by ~30%.

The truss model was not able to accurately predict stiffness in the small-deflection region as it neglects the bending deformation, which dominates energy storage at small deflections. The truss model is better able to predict stiffness at large-displacement as the axial stiffness of the CNTs dominates stiffness at large deflections.

The accuracy of the PRBM is sensitive to the value of γ. Figure 8 shows that changing γ from 0.85 to 0.91 reduces the maximum error from 12.7% to 2.7%. This higher value of γ is consistent with the fact that flexible elements have a higher γ when subjected to tensile loads [8]. The choice of K_θ has a modest impact on accuracy. When K_θ increases by 5%, the maximum error increases from 12.7% to 13.4%. For large displacements, over 90% of the applied force works to axially deform the CNTs. As K_θ does not appear in the axial stiffness section of Eq. (8), its impact is expected to be modest. The preceding is for a (5,5) SWCNT. Other chiralities are a subject of future study.

Table 1 PRBM parameter values

$(EA)_{\text{axial}}$	514.4 nN [14]
$(EI)_{\text{bending}}$	35.68 nN nm^2 [14]
γ	0.85 [9]
K_θ	2.65 rad^{-1} [9]
L_o	7.64 nm
D_o	0.678 nm
t	0.075 nm [14]
v	0.28 [19]

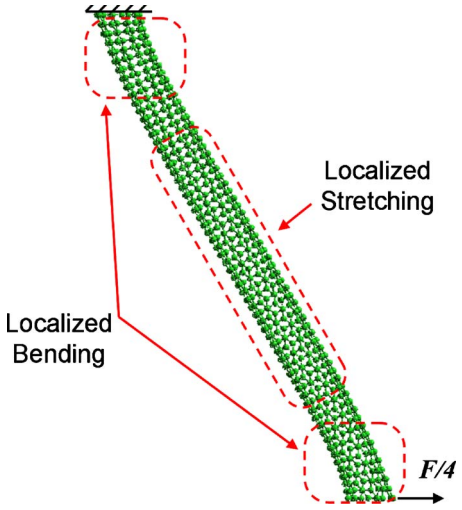

Fig. 7 Zones of deformation in one CNT beam

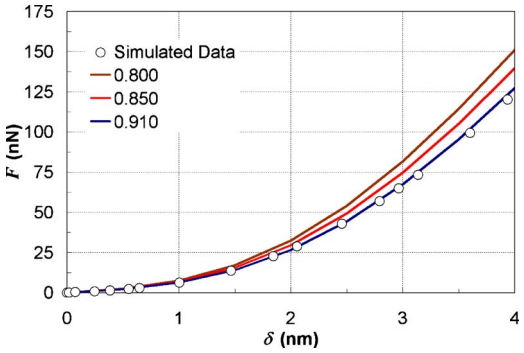

Fig. 8 Effect of γ on the elastomechanic response

7 Conclusion

Our adapted PRBM provides a means to predict the large, nonlinear deflections of fixed-clamped CNTs. For a (5,5) CNT, a properly tuned PRBM exhibits less than 3% error from molecular simulations of CNT deflections in contrast to 91% error from the traditional models. This PRBM is envisioned to open the door to rapid modeling and design of new CNT-based mechanisms. Recent work in the design of CNT resonators [20] and CNT radio frequency NEMS switches [5] requires high strain mechanical models of CNTs for which the PRBM is ideally suited.

References

[1] Ekinci, K., 2005, "Electromechanical Transducers at the Nanoscale: Actuations and Sensing of Motion in Nanoelectromechanical Systems (NEMS)," Small, **1**(8–9), pp. 786–797.

[2] Stampfer, C., Jungen, A., Linderman, R., Obergfell, D., Roth, S., and Hierold, C., 2006, "Nano-Electromechanical Displacement Sensing Based on Single-Walled Carbon Nanotubes," Nano Lett., **6**(7), pp. 1449–1453.

[3] Witkamp, B., Poot, M., and van der Zant, H. S. J., 2006, "Bending-Mode Vibration of a Suspended Nanotube Resonator," Nano Lett., **6**(12), pp. 2904–2908.

[4] Rueckes, T., Kim, K., Joselevich, E., Tseng, G., Cheung, C., and Lieber, C., 2000, "Carbon Nanotube-Based Nonvolatile Random Access Memory for Molecular Computing," Science, **289**(5476), pp. 94–97.

[5] Dragoman, M., Takacs, A., Muller, A. A., Hartnagel, H., Plana, R., Grenier, K., and Dubuc, D., 2007, "Nanoelectromechanical Switches Based on Carbon Nanotubes for Microwave and Millimeter Waves," Appl. Phys. Lett., **90**, p. 113102.

[6] Yu, M.-F., Files, B., Arepalli, S., and Ruoff, R., 2000, "Tensile Loading of Ropes of Single Wall Carbon Nanotubes and Their Mechanical Properties," Phys. Rev. Lett., **84**(24), pp. 5552–5555.
[7] Lu, J., and Zhang, L., 2006, "Analysis of Localized Failure of Single-Wall Carbon Nanotubes," Comput. Mater. Sci., **35**, pp. 432–441.
[8] Howell, L. L., 2001, *Compliant Mechanisms*, Wiley, New York.
[9] DiBiasio, C., Culpepper, M., Panas, R., Howell, L., and Magleby, S., 2008, "Comparison of Molecular Simulation and Pseudo-Rigid-Body Model Predictions for a Carbon Nanotube-Based Compliant Parallel-Guiding Mechanism," ASME J. Mech. Des., **130**(4), p. 042308.
[10] Ke, C., Espinosa, H. D., and Pugno, N., 2005, "Numerical Analysis of Nanotube Based NEMS Devices—Part II: Role of Finite Kinematics, Stretching and Charge Concentrations," ASME J. Appl. Mech., **72**(5), pp. 726–731.
[11] Saito, R., Dresselhaus, G., and Dresselhaus, M. S., 2005, *Physical Properties of Carbon Nanotubes*, Imperial College Press, London.
[12] Pantano, A., Parks, D. M., and Boyce, M. C., 2004, "Mechanics of Deformation of Single and Multi-Wall Carbon Nanotubes," J. Mech. Phys. Solids, **52**, pp. 789–821.
[13] Qian, D., Wagner, G. J., Liu, W. K., Yu, M.-F., and Ruoff, R. S., 2002, "Mechanics of Carbon Nanotubes," Appl. Mech. Rev., **55**(6), pp. 495–533.
[14] DiBiasio, C., Cullinan, M., and Culpepper, M., 2007, "Difference Between Bending and Stretching Moduli of Single-Walled Carbon Nanotubes That are Modeled as an Elastic Tube," Appl. Phys. Lett., **90**(20), p. 203116.
[15] Culpepper, M., DiBiasio, C., Panas, R., Magleby, S., and Howell, L., 2006, "Simulation of a Carbon Nanotube-Based Compliant Parallel-Guiding Mechanism: A Nanomechanical Building Block," Appl. Phys. Lett., **89**(20), p. 203111.
[16] Doyle, J., 2001, *Nonlinear Analysis of Thin-Walled Structures: Statics, Dynamics, and Stability*, Springer, New York.
[17] Senturia, S., 2002, *Microsystem Design*, 1st ed., Kluwer Academic, Boston, MA, p. 252.
[18] Leach, A. R., 2001, *Molecular Modeling*, 2nd ed., Prentice Hall, Harlow, England.
[19] Lu, J., 1997, "Elastic Properties of Carbon Nanotubes and Nanoropes," Phys. Rev. Lett., **79**(7), pp. 1297–1300.
[20] Ouakad, H. M., and Younis, M. I., 2010, "Nonlinear Cynamics of Electrically actuated Carbon Nanotube," ASME J. Comput. Nonlinear Dyn., **5**(1), p. 011009.